

Observing coherence: The mode volume of D=3 dimensional random lasers

Andreas Lubatsch^{1,2} and Regine Frank^{2,3*}

¹ *Georg-Simon-Ohm University of Applied Sciences, Keßlerplatz 12, 90489 Nürnberg, Germany*

² *Physikalisches Institut, Rheinische Friedrich-Wilhelms Universität Bonn, Wegelerstr. 8, 53115 Bonn, Germany*

³ *Serin Physics Laboratory, Department of Physics and Astronomy, Rutgers University, 136 Frelinghuysen Road, Piscataway, NJ 08854-8019, USA*

(Dated: December 8, 2024)

We present photonic transport in D=3 dimensional granular dissipative semiconductor media. Our self-consistent diagrammatic approach of the Bethe-Salpeter equation including the Cooperon predicts a spatially dependent correlation volume within the disordered medium that is equivalent to the laser's mode extent inside the sample. Our results are relevant for the construction of disordered complex semiconductor micro-lasers and active Mie sphere samples. They define concrete critical parameters for the phase transition to lasing in disordered non-linear random media.

PACS numbers: 42.25.Dd, 42.25.Hz, 42.55.Zz

Light transport in disordered nonlinear random media is a fascinating subject that culminates in research of random lasers [1–5], DFB lasers [6] and nonlinear optical fibres [7]. If these systems can be operated spectrally and spatially controlled they are featuring a future as large area coherent light sources ahead of all state of the art LEDs. Theoretically D=3 dimensional random lasers in finite dimensions confront scientists usually with tremendous computational efforts. Within extended granular systems this can only be reached by novel approaches of quantum field theory [8]. Expanding them to photonics [9] and to light transport in matter under strong magnetic fields [10] is the aim of high-performance numerical physics. In this letter we develop the first theory that is able to describe the modal behavior of random lasers. The electrodynamics for transport in non-linear media is described basically by the wave equation for Kerr-Media

$$\Delta \vec{E} - \frac{\epsilon}{c^2} \frac{\partial^2 \vec{E}}{\partial t^2} = \frac{1}{c^2 \epsilon_0} \frac{\partial^2 \vec{P}}{\partial t^2}. \quad (1)$$

where the polarizability $\vec{P}(\vec{E})$ may be decomposed in linear and non-linear part $\vec{P}(\vec{E}) = \epsilon_0(\epsilon - 1)\vec{E} + \vec{P}_{NL}$. The electric displacement inside a medium is written as $\vec{D}(\vec{E}) = \epsilon_0\epsilon\vec{E} + \vec{P}_{NL}$. Kerr media are $\chi^{(2)}$ or higher order processes in their dependency to the electrical field E .

$$\vec{P} = \epsilon_0\chi^{(1)}\vec{E} + \epsilon_0\chi^{(2)}\vec{E} \cdot \vec{E} + \dots \quad (2)$$

We describe the formalism yielding the extended Bethe-Salpeter equation Fig.1 and lasing in steps (I) the interaction of the light wave with the single independent scatterer, (II) the propagation of the light wave in disordered random media, (III) the propagation with respect to the intensity correlation and interference effects and (IV) lasing.

The propagating wave is described by the single-particle Green's function Eq.(3) solving the non-linear wave equation.

$$G_{\vec{k}}^{\omega} = \frac{1}{\epsilon_b(\omega/c)^2 - |\vec{k}|^2 - \Sigma_{\vec{k}}^{\omega}} \quad (3)$$

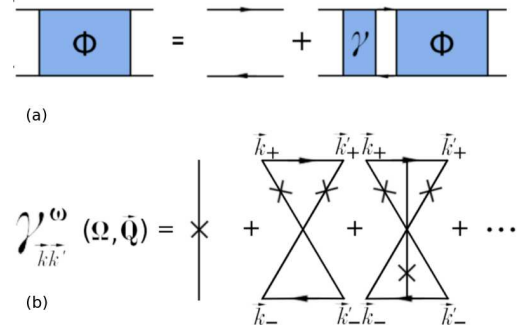


FIG. 1: (a) Schematic representation of the Bethe-Salpeter equation. (b) Irreducible vertex including all orders of most crossed diagrams (Cooperon) which represents all quantum-coherent interference contributions in presence of disorder.

The granularity of the medium (I) as well as its randomness are implemented as spatially dependent potential of the permittivity $\epsilon_s(\vec{r})$. The order of non-linearity is a matter of the numerical selfconsistency as the independent semiconductor scatterers [11] are well described by the T-matrix [12, 13] for spherical Mie particles including the self-consistent complex refractive index.

We use in presence a model of independent Mie scatterers Fig.2 for the self-energy contribution $\Sigma_{\vec{k}}^{\omega}$. Originally [14, 15] the Mie scattering coefficients of n-th order read

$$a_n = \frac{m\Psi_n(my)\Psi'_n(y) - \Psi_n(y)\Psi'_n(my)}{m\Psi_n(my)\xi'_n(y) - \xi_n(y)\Psi'_n(my)} \quad (4)$$

$$b_n = \frac{\Psi_n(my)\Psi'_n(y) - m\Psi_n(y)\Psi'_n(my)}{\Psi_n(my)\xi'_n(y) - m\xi_n(y)\Psi'_n(my)}.$$

In this notation $m = \frac{n_s}{n_b}$ is the relative refractive index between scatterer and background, $y = \frac{2\pi n_s r_S}{\lambda}$ is the size parameter depending on the scatterers' radius r_S as well as the transport wavelength λ . Ψ_n, ξ_n are Riccati-Bessel functions. The refractive index $n_s(\Phi)$ inherits a higher-order non-linearity as consequence of the selfconsistency $\text{Im}\epsilon_s(\Phi)$. The independent scatterer approach works very

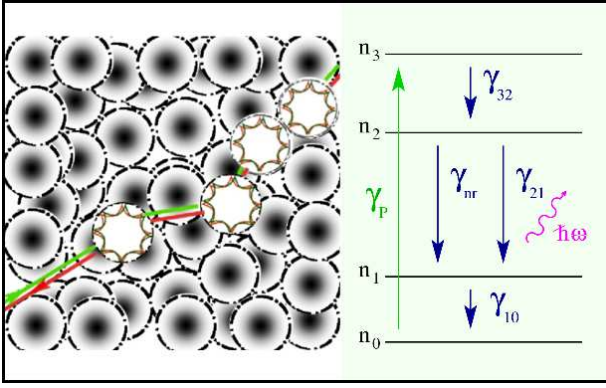


FIG. 2: (Left) Sketch of a disordered semi-conductor random laser slab open in z -direction. Photonic transport processes (red) and their time reversal (green) and internal resonances within independent Mie scatterers. (Right) 4-level laser rate equation scheme. Sinuous lines are electronic procedures, 2-photon pumping (green), spontaneous γ_{32} and spontaneous emission γ_{sp} , stimulated emission γ_{21} , $\hbar\omega$ represents lasing.

well in dense random media of filling of 35% – 55%. The inter-scatterer dynamics is effectively mapped on the dynamical $n_s(\Phi)$ and non-linear response even though we use the far field description of Mie scattering.

The wave field Ψ_ω solves (II) the wave equation Eq. (1) and builds up the intensity field $\Phi_{\vec{k}\vec{k}'}^\omega(\vec{Q}, \Omega)$ in the sample. The four point correlator $\Phi_{\vec{k}\vec{k}'}^\omega(\vec{Q}, \Omega) = \langle \hat{G}_{\vec{k}_+ \vec{k}_+}^R(\omega) \hat{G}_{\vec{k}_- \vec{k}_-}^A(\omega) \rangle$ expressed in terms of retarded and advanced Green's function $\hat{G}^{R/A}$ denoting the field and its time-reversal. We utilize the transformation of coordinates in center-of-motion (\vec{Q}, Ω) and relative (\vec{k}, ω) momenta and frequencies [16] $\vec{k}_\pm = \vec{k} \pm \vec{Q}/2$ and $\omega_\pm = \omega \pm \Omega/2$. Considering the slab geometry extended within the (x, y) -plane and finite in z -direction, the full Fourier transform as indicated in infinite samples [17] is replaced by a partial Fourier transform following the argument of scale separation for field Ψ and intensity Φ . Ψ is characterized by the wavelength λ whereas change of the light intensity Φ is characterized with the transport mean free path ξ derived in due course of the paper. In (x, y) -plane the standard Fourier transform is used, in the limited z -direction we Fourier transform the relative coordinate but the center-of-motion coordinate Z remains as is.

Applying the same arguments (III) to the equation of motion for the intensity correlation, known as Bethe-Salpeter equation $\Phi_{\epsilon\epsilon} = G^R G^A [1 + \int \frac{d^3k}{(2\pi)^3} \gamma \Phi_{\epsilon\epsilon}]$, we obtain the Boltzmann or kinetic equation for transport Eq.(6), where we introduced the following abbreviations, also for later use, $\Delta\Sigma = \Sigma^A(\omega_-) - \Sigma^R(\omega_+)$, $\square\Sigma = \Sigma^A(\omega_-) + \Sigma^R(\omega_+)$, and equivalent expressions for $\Delta G_{\vec{k}\vec{k}'}^{\omega-}$ and $\square G_{\vec{k}\vec{k}'}^{\omega-}$. The term $\gamma_{\vec{k}\vec{k}'}^\omega(Z, Z'', \vec{Q}_\parallel, \Omega)$ is the irreducible vertex representing coherent photonic interaction in the disordered granular non-linear system. The Ward identity, here for laser active, complex refractive Mie scatterers, ensures local energy conservation [13]. The solution to Eq.(6), is derived to be the energy density response $\Phi_{\epsilon\epsilon}$ in its diffusion pole structure Eq.(5)

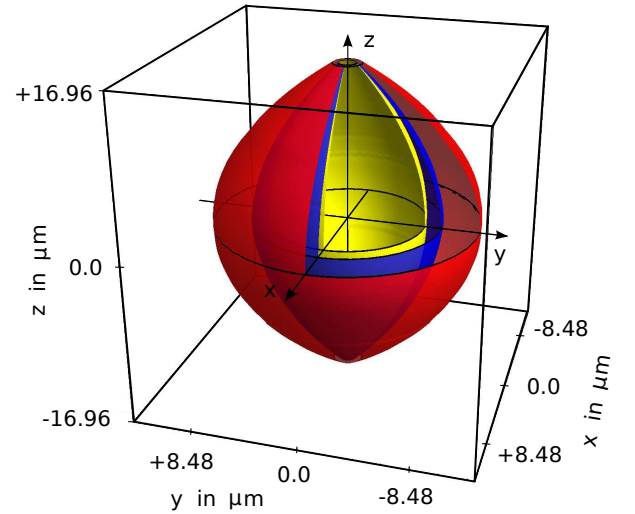


FIG. 3: Coherence volume within a D=3 dimensional random laser slab of ZnO particles. Scatterers' radius is $r = 212 \text{ nm}$, the real part of permittivity $\text{Re}\epsilon_s = 4.0164$, the transport wavelength is $\lambda = 385 \text{ nm}$. The strongly scattering medium of monodisperse ZnO Mie spheres is open and lossy in the z -direction. Pump rate $P = 1$ (red), 3 (blue), 5 (yellow) in units of $1/\gamma_{21}$. The stationary state marks the laser threshold.

$$\Phi_{\epsilon\epsilon} = \frac{N_\omega}{\Omega + iDQ_\parallel^2 + iD\xi^{-2}}. \quad (5)$$

$$\begin{aligned} [2\text{Re}(\epsilon_b)\omega\Omega - 2\vec{k}_\parallel \cdot \vec{Q}_\parallel + 2ik_z\partial_Z + \Delta\Sigma - \Delta\epsilon_b\omega^2] \Phi_{\vec{k}\vec{k}'}^\omega(Z, Z', \vec{Q}_\parallel, \Omega) \\ = \Delta G\delta(\vec{k} - \vec{k}') + \sum_{Z''} \Delta G \int \frac{d^3k''}{(2\pi)^3} \gamma_{\vec{k}\vec{k}''}^\omega(Z, Z'', \vec{Q}_\parallel, \Omega) \Phi_{\vec{k}''\vec{k}'}^\omega(Z'', Z', \vec{Q}_\parallel, \Omega) \end{aligned} \quad (6)$$

$$M(\Omega) = \frac{1}{\int \frac{d^3k}{(2\pi)^3} (2\vec{k} \cdot \hat{Q})(\Delta G)^2} \int \frac{d^3k}{(2\pi)^3} \int \frac{d^3k'}{(2\pi)^3} (2\vec{k} \cdot \hat{Q}) \Delta G_k \gamma_{kk'} (2\vec{k}' \cdot \hat{Q}) (\Delta G_{k'})^2 \quad (7)$$

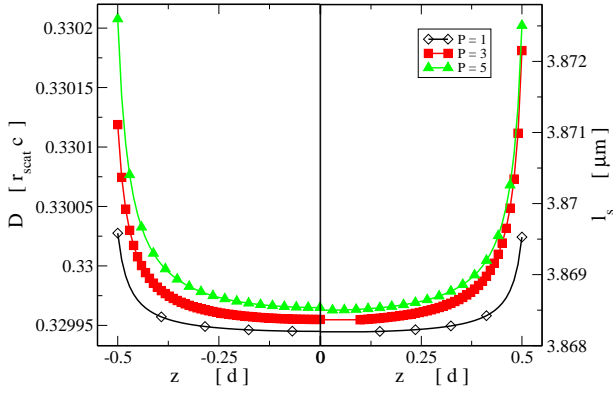


FIG. 4: *Left panel:* Indepth dependent diffusion constant $D(\Omega = 0; Z)$. *Right panel:* Indepth dependent scattering mean free path $l_s = \frac{1}{2\text{Im}[\sqrt{q^2 + i\text{Im}\Sigma(\omega)}]}$. Both quantities show differing behavior at the samples borders $\pm 0.5d$.

We define the correlation length ξ depending on the energy density $\Phi_{\epsilon\epsilon}$ itself

$$\frac{1}{\xi^2(Z)} = \frac{N_\omega}{D(\Omega = 0; Z)\Phi_{\epsilon\epsilon}(Q_{||} = 0, Z; \Omega = 0)}. \quad (8)$$

Here the full diffusion constant $D(\Omega = 0; Z)$ is derived according to $D(\Omega) = D_0^{tot} - \tau^2 D(\Omega)M(\Omega)$ where bare diffusion $D_0 = \frac{2v_E c_p}{\omega \Delta G} \int \frac{d^3 k}{(2\pi)^3} (\vec{k} \cdot \hat{Q})^2 \Delta G$ is complemented by terms originating from the active medium as the scatterers $D_s = \frac{1}{8} r_\epsilon A_\epsilon \tau^2 \tilde{D}_0$ or the background $D_b = \frac{1}{4} (\omega\tau)^2 \Delta\epsilon_b \tilde{D}_0$. So the diffusion constant without memory effects reads $D_0^{tot} = D_0 + D_s + D_b$. The last term $-\tau^2 D(\Omega)M(\Omega)$ contains the memory kernel $M(\Omega)$, Eq.(7), that bares the Cooperon contribution and consequently all interferences. \tilde{D}_0 equals D_0 where the imaginary part ΔG replaced by the real part $\square G$. The renormalized density of states LDOS is derived to be

$$N_\omega = \frac{\omega^2 \Delta G_0(\vec{Q}, \Omega)}{c_p^2 g_\omega^{(1)} [1 + \Delta(\omega)]}. \quad (9)$$

We use the notation and the abbreviations of [16]. $\Delta(\omega) = B_\epsilon A_\epsilon + i r_\epsilon \partial_\Omega A_\epsilon(\Omega)$ with $A_\epsilon = 2[u_\epsilon \text{Re} G_o + \text{Re} \Sigma_o]$ and $B_\epsilon = \frac{(\text{Re} \Delta\epsilon)^2 + (\text{Im} \Delta\epsilon)^2}{2\omega^2 (\text{Re} \Delta\epsilon)^2}$, ∂_Ω is the differential resulting from the expansion in \vec{Q} and Ω . This includes the momentum integrated ΔG to be $\Delta G_0 = \int \frac{d^3 k}{(2\pi)^3} \Delta G_p^\omega(Q, \Omega, Z)$ and $\Delta\epsilon = \epsilon_s - \epsilon_b$, $u_\epsilon = \frac{\text{Im}(\Delta\epsilon \Sigma_\omega)}{\text{Im}(\Delta\epsilon G_\omega^\omega)}$ and $r_\epsilon = \text{Im} \Delta\epsilon / \text{Re} \Delta\epsilon$ and $g_\omega^{(1)} = \frac{4\omega}{c^2} \text{Re} \epsilon_b$, for completeness $g_\omega^{(0)} = \frac{2\omega}{c^2} \text{Im} \epsilon_b$. $v_E = \frac{c^2}{c_p \text{Re} \epsilon_b} \frac{1}{1 + \Delta(\omega)}$ is the energy transport velocity, whereas $c_P = \text{Re} \frac{c}{\sqrt{\epsilon_b - \Sigma_o^\omega \frac{c^2}{\omega^2}}}$ equals the phase velocity, each selfconsistently derived. The time scale τ is discussed in detail in [16].

$$iD\xi^{-2} = -iD\chi_d^{-2} - c_1 \left(\partial_Y^2 \Phi_{\epsilon\epsilon}(Q, \Omega) \right) + c_2. \quad (10)$$

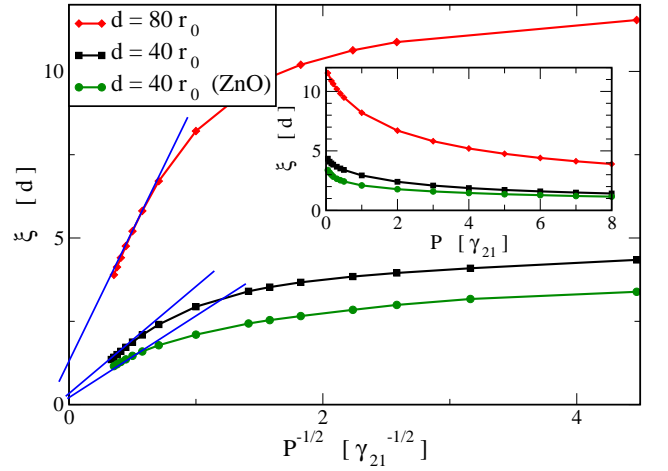


FIG. 5: Selfconsistent coherence length ξ for various thicknesses d of the random laser slab. Towards strong pumping P a transition to a power law behavior of ξ with $1/\sqrt{P}$ is found. Results are for identical $r_s = 212 \text{ nm}$ of ZnO ($n = 2.0041$) and C (diamond, $n = 2.4$). Diamond at transport wavelength $\lambda = 385 \text{ nm}$ is significantly closer to the Mie resonance.

By solving (IV) the renormalized diffusion equation Eq.(10) coupled to the 4-level laser rate equations [18, 19] the coefficients c_1 and c_2 are selfconsistently derived, and we arrive the spatial distribution of energy density:

$$-\frac{\partial^2}{\partial Y^2} \Phi_{\epsilon\epsilon} = \frac{1}{D} \frac{D}{-\chi_d^2} \Phi_{\epsilon\epsilon} + \text{ASE}. \quad (11)$$

The nonlinear self-consistent microscopic random laser gain $\gamma_{21} n_2$ incorporates the influence of the boundary renormalized length scale χ_d, γ_{21} is the transition rate from laser level 2 to level 1, n_2 is the electronic occupation number of level 2. This yields the inversion condition

$$\frac{D}{-\chi_d^2} = \gamma_{21} n_2 \quad (12)$$

in stationary state. χ_d is the length scale implicated by dissipation in the bulk alone. The modification of the boundary specifies the relation between lasing emission and amplified spontaneous contributions (ASE), Eq.(11), relevant for light emitting diodes (LEDs).

As results, we find a large set of selfconsistent scales, e.g. the diffusion constant D the scattering mean free path l_s the transport mean free path or coherence length ξ , the energy transport velocity v_E as well as the phase velocity c_p , the energy and intensity dependent LDOS N_ω , the intensity correlator including interference influences $\Phi_{\epsilon\epsilon}$ as well as the laser thresholds and the gain in stationary state. Our results for the energy transport velocity v_e and the phase velocity c_p in connection to the LDOS N_ω Eq.(9) are discussed in following up work with respect to sub- and hyper-diffusion.

As the central result in this paper we derive the D=3 dimensional pump intensity dependent coherence volume

Fig. 3 resulting from the coherence scale ξ which is displayed dependent to the samples depth. The inherent differential in Eq.(10) is technically extremely pronounced in the decrease of coherence in Fig. 3. This result is novel in theory. First it is obvious that the mode loses coherence near the samples open surfaces (z-direction) but it is striking that a huge coherent transport mean free path ξ can be built up in the samples center of about $16,96 \mu\text{m}$ which is about factor 5 of the scattering mean free path and about 45-times larger than the wavelength of 385 nm . This length is a direct measure of the Cooperon contribution, which is the fully coherent photon and its time reversal procedure [20] in the intensity correlator $\Phi_{\epsilon\epsilon}$ that acts as the stimulation process of coherent emission. This contribution suffers due to boundary effects that are position dependent whereas the monodisperse scatterers' nonlinearity decreases its amount homogeneously. It is emphasized that coherent emission as in the laser in stationary state is different from purely multiple scattered light, even though including nonlinearities [21]. Consequentially the transport mean free path ξ in [17] is formally equivalent to the here derived correlation length ξ , however its physical meaning is fundamentally different. This is actually seen in the experiment by measuring second order (temporal) coherence in a Michelson experiment [22].

The second main result of this paper is, that in stationary state coherence decreases with increasing pump strength P whereas for comparison the selfconsistent diffusion constant D and the scattering mean free path l_s , Fig. 4, express an inverse behavior. While diffusion is increased, localization (Cooperon contribution) is definitely decreasing, and the scattering mean free path l_s is large for enhanced pumping P , near the samples boundaries [18, 19] but even more in the bulk of the sample. We expect these findings to be measured in close up experiments soon. Good candidates are quasi $D = 1$ or $D = 2$ dimensional disordered photonic crystals [23–26] disorder is fairly controlled and measurement access is given from distinct directions correlated to pure transport or out-of-plane scattering and emission. Also spatially varying gain is realizable in a controlled way [27].

Qualitatively equal but inverted is the effect definitely present on a scale much smaller than the wavelength λ in the depth-dependent behavior of the diffusion constant D as well as the scattering mean free path l_s Fig. 4. This confirms first estimations of boundaries in earlier work by Akkermans *et al.* [28] on Anderson localization. However the result in Fig. 3 can not be derived if the difference due to boundaries would be neglected. We emphasize that homogeneous loss as it has been considered in [29] will certainly not yield comparable results.

In Fig. 5 we discuss the coherence length ξ and its transition from linear behavior to power law for identical particles of the refractive index of ZnO and C (diamond) with scatterer radius $r_s = 212 \text{ nm}$. The particle

size is comparable to the wavelength $\lambda = 385 \text{ nm}$. The results for diamond are closer to the Mie resonant case. Consequentially the same pumping results in higher laser efficiency and an increasing n_{ph} , but also in a larger coherence length ξ which is found in Fig. 5. The importance of the Mie resonator [30, 31] as such is underlined by these findings, even though we are still far off the actual resonant case. In recent work on non-equilibrium dynamics in ZnO Mie resonators the extreme influence of the resonance on the life times of electronic states, optical conductivity and consequentially gain is shown [32]. In our considerations here, we estimate quasi-stationary pumping, so it is expected that for the ultrafast regime the effect will play even a bigger role for the dwell times [33] and the laser thresholds.

Our results of numerical fit-parameter free Vollhardt-Wölfle theory suggest that boundaries significantly renormalize the modes of random lasers, specifically indepth of the random laser sample. A mode volume is created on average which will result in an equivalent spectrum in the measurement. This volume is a characteristic length scale for the random laser construction. Furthermore we find the inverse behavior between the characteristic quantities D, l_s on the one hand and the coherence length ξ on the other. We built our framework in this paper on the scalar non-linear wave-equation, which is a fairly good approximation for particles going towards the Rayleigh case in homogeneous randomized samples. It will be subject of future work to discuss the influence of gain and absorption with respect to sub- and hyper-diffusion. With respect to quasi-order and *meta glasses* of complex resonant particles and coated spheres it will be interesting to investigate the selfconsistent relation between non-linearity and the optical angular momentum (OAM) for light transport as well as random lasing in stationary state. The full vector wave description leads to matrix Green's functions and requires a more sophisticated Ward identity to ensure energy conservation.

Acknowledgment: We thank H. Cao, B. Shapiro, H. Kalt, K. Busch, J. Kroha and R. v. Baltz for discussions. RF gratefully acknowledges the DAAD for financial support.

* Correspondence should be addressed to: frank@physics.rutgers.edu

- [1] H. Cao *et al.*, *Phys. Rev. Lett.* **82**, 2278-2281 (1999).
- [2] M. A. Noginov *et al.*, *Nature* **460**, 1110-1112 (2009).
- [3] R. C. Polson, Z. V. Vardeny, *Optics Letters*, **35**, 16, 2801 (2010).
- [4] G. Hackenbroich, C. Viviescas, F. Haake, *Phys. Rev. Lett.*, **89**, 083902 (2002).
- [5] G. Hackenbroich, *J. of Phys. A: Math. Gen.*, **38**, 10537 (2005).
- [6] J. Faist *et al.*, *Science* **264** (5158) 553-556 (1994).

- [7] S. K. Turitsyn *et al.*, *Nature Photonics* **4** 231-235 (2010).
- [8] D. Vollhardt, P. Wölffe, *Phys. Rev. B* **22**, 4666 (1980).
- [9] B. A. van Tiggelen, *Phys. Rev. Lett.* **91** 243904 (2003).
- [10] B. A. van Tiggelen, *Phys. Rev. Lett.* **75** 422-424 (1995).
- [11] A. Lagendijk, B. A. van Tiggelen, *Physics Reports* **270** 143-215 (1996).
- [12] H. T. Nieh, L. Chen, P. Sheng, *Phys. Rev. E* **57**, 1, 1145 (1998).
- [13] A. Lubatsch, J. Kroha, K. Busch, *Phys. Rev. B* **71**, 184201 (2005).
- [14] G. Mie, *Annalen der Physik*, **4**, 25, 377-445 (1908).
- [15] C. F. Bohren, D. R. Huffman, *Absorption and Scattering of Light by Small Particles*, Wiley-VCH, ISBN-13: 978-0471293408 (2013).
- [16] R. Frank, A. Lubatsch, *Phys. Rev. A* **84**, 013814 (2011).
- [17] R. Frank, A. Lubatsch, J. Kroha, *Phys. Rev. B* **73**, 245107 (2006).
- [18] A. Lubatsch, R. Frank, *New J. Phys.* **16**, 083043 (2014).
- [19] A. Lubatsch, R. Frank, arXiv:1505.06781, Scientific Reports (accepted).
- [20] L. Onsager, *Phys. Rev.* **37**, 405426 (1931), *Phys. Rev.* **38**, 2265 (1931).
- [21] G. Maret, T. Sperl, W. Buehrer, A. Lubatsch, R. Frank, C. M. Aegerter, *Nature Photonics* **7**, 934-935 (2013).
- [22] B. Redding, M. A. Choma, H. Cao, *Opt. Lett.* **36** 17 3404 (2011).
- [23] J. Liu *et al.*, *Nature Nanotechnology* **9**, 285-289 (2014).
- [24] A. K. Tiwari, S. Mujumdar, *Phys. Rev. Lett.* **111**, 233903 (2013).
- [25] R. Uppu, S. Mujumdar, *Phys. Rev. Lett.* **114** 183903 (2015).
- [26] M. Renner, G. von Freymann, *Advanced Optical Materials* **2**, 3, 226-230 (2014).
- [27] J. E. G. J. Wijnhoven, W. L. Vos, *Science* **281**(5378): 802-4, 1998).
- [28] E. Akkermans, P. E. Wolf, R. Maynard, *Phys. Rev. Lett.* **56**, 1471 (1986).
- [29] D. Wiersma, *Nature Physics* **4**, 359-367 (2008).
- [30] K. L. van der Molen *et al.*, *Opt. Lett.* **31**, 1432 (2006).
- [31] N. Yamamoto, S. Ohtani, F. J. Garcia de Abajo, *Nano Lett.* **11**, 91-95 (2011).
- [32] A. Lubatsch, R. Frank, arXiv:1504.00949 (2015).
- [33] B. A. van Tiggelen, A. Tip, A. Lagendijk, *J. Phys. A Math. Gen.* **26** 1731-1748 (1993).